Faceted–nonfaceted growth transition and 3-D morphological evolution of primary Al_6Mn microcrystals in directionally solidified Al–3 at.% Mn alloy

Huijun Kang and Tongmin Wang[a)]
Department of Materials Engineering, School of Materials Science and Engineering, Dalian University of Technology, Dalian 116024, China

Xinzhong Li, Yanqing Su, Jingjie Guo, and Hengzhi Fu
Department of Materials Engineering, School of Materials Science and Engineering, Harbin Institute of Technology, Harbin 150001, China

(Received 27 February 2014; accepted 1 May 2014)

A comprehensive understanding of the growth pattern of intermetallic compounds (IMCs) during solidification is critical to both the crystal-growth theory and its property optimization. In this article, growth pattern and three-dimensional (3D) morphology of primary Al_6Mn IMC were investigated in directionally solidified Al–3 at.% Mn alloy at a wide range of growth rates. A transition from faceted (<60 μm/s) to nonfaceted growth (>100 μm/s) was observed with increasing growth rates. Correspondingly, 3D morphologies of primary Al_6Mn change from a solid polyhedron to a hollow structure, and then to a dendrite. This kind of change is associated with the competitive growths of different crystal planes determined by the crystallographic anisotropy and growth kinetics of Al_6Mn. A growth model based on atomic cluster attachment is proposed to reveal the growth transition, and a growth-rate ratio between different crystal planes is used to appropriately reveal the formation mechanism of different morphologies at low rates.

I. INTRODUCTION

The melt-growth control of intermetallic compounds (IMCs) is of practical interest because of the significance of IMCs with appropriate morphologies, sizes, distributions, and volume fractions introduced in alloys for optimizing properties.[1–6] However, IMCs exhibiting complex crystal structure and directional bonding commonly show a faceted growth with a strong anisotropy during solidification.[7,8] Growth discrepancies of different crystal planes, originated from the inherent crystal structure and external environment, usually lead to complicated morphologies of IMCs. Especially, a potential transition is predicted theoretically from faceted IMCs to nonfaceted IMCs then quasicrystals or noncrystals with increasing cooling rates.[9,10] However, further accumulation of experimental evidences is required for understanding the detailed pattern formation of melt-growth IMCs.

Several attempts[7,8,11–15] have been made for this purpose. For instance, deep-etching and extracting techniques were used to characterize the three-dimensional (3D) morphologies of primary Al_3Sc IMCs in casting aluminum–scandium (Al–Sc) alloys.[11] The growth of primary Mg_2Si IMCs in casting aluminum–magnesium–silicon (Al–Mg_2Si) alloys was highly dependent on its crystal structure and growth conditions.[7] Recently, we have investigated the 3D morphologies of Al_6Mn IMCs at a growth rate of 1 μm/s in directionally solidified Al–3 at.% Mn alloys.[8] It is found that directional solidification is an appropriate technique to reveal the growth of IMCs due to the defined conditions of crystal growth. In this article, further efforts have been made to clarify potential growth transition of Al_6Mn IMCs from faceted to nonfaceted growth with increasing growth rates and to explain the various faceted growth morphologies by a growth-rate ratio between different crystal planes. Al_6Mn IMC is the most common stable phase in Al–Mn system alloys which has significant effects on the performance of these alloys. For investigating the faceted–nonfaceted growth transition and 3D morphological evolution of primary Al_6Mn microcrystals, we select a typical off-eutectic-type alloy (Al–3 at.% Mn alloy) as a model alloy in this study.

II. MATERIALS AND METHODS

Al–3 at.% Mn master ingot was prepared by induction melting aluminum (99.9 wt.%) and manganese (99.9 wt.%) under an argon atmosphere. The as-cast samples with size of D3 mm × 110 mm were obtained from the ingot by electrical discharge machining. The samples were placed into a high purity alumina tube of 3.5 mm inner diameter, which was connected with a motor. Then the sample was pulled at growth rates of (1–1000 μm/s) after initial melting and thermal stabilization together with alumina tube.

a)Address all correspondence to this author.
e-mail: tmwang@dlut.edu.cn
DOI: 10.1557/jmr.2014.111

After a growth distance of 30 mm, the samples were quenched into the gallium–indium–tin (Ga–In–Sn) liquid alloy to preserve the solid–liquid interface. Temperature profiles were measured separately using a PtRh30-PtRh6 thermocouple inserted within a fine alumina tube (0.6 mm internal diameter) down to the center of the samples. During the pulling process, the thermocouple moved downwards with the sample at the same pulling rate. The temperature gradient can be calculated from the measured temperature profiles and is estimated about 25 ± 0.5 K/mm in the present work.

The microstructure was characterized by scanning electron microscope (SEM; Model No. SEM-Quanta 200FEG, FEI Company, Hillsboro, OR). Primary Al_6Mn IMCs and its structure were identified by transmission electron microscopy (TEM; Model No. TEM-TECNAI F30, FEI Company, Hillsboro, OR). The samples for TEM observation were prepared by a standard combination of mechanical and ion-beam thinning techniques. An etchant of NaOH-aqueous solution was used to dissolve the eutectic matrix and preserve Al_6Mn IMCs whose 3D morphologies were characterized by secondary electron image.

III. RESULTS AND DISCUSSION

A. Microstructures in directionally solidified Al–3 at.% Mn alloy

Figure 1(a) shows the structure of directionally solidified Al–3 at.% Mn alloy at a typical growth rate of 10 μm/s. Lath-like Al_6Mn IMCs (bright contrast) are preferentially aligned to the growth direction and distributed into the (Al + Al_6Mn) eutectic matrix (dark contrast). The quenching interface reveals that primary Al_6Mn first precipitates from melt, followed by an eutectic reaction during solidification of Al–3 at.% Mn alloy, as expected in Al–Mn binary diagram.[16] Al_6Mn IMCs display faceted morphologies with planar, angular surfaces, and diverged tips. Figure 1(b) shows the TEM image of the mixture of Al_6Mn and Al solid solution. A sharp interface appears without observable diffusion layer between them. It may be attributed to the fact that Al_6Mn is a typical ionic compound with a strict stoichiometric ratio.[17] The corresponding selected area diffraction pattern of Al_6Mn in Fig. 1(c) confirms its orthorhombic structure with lattice parameters of a = 0.7545 nm, b = 0.6490 nm, and

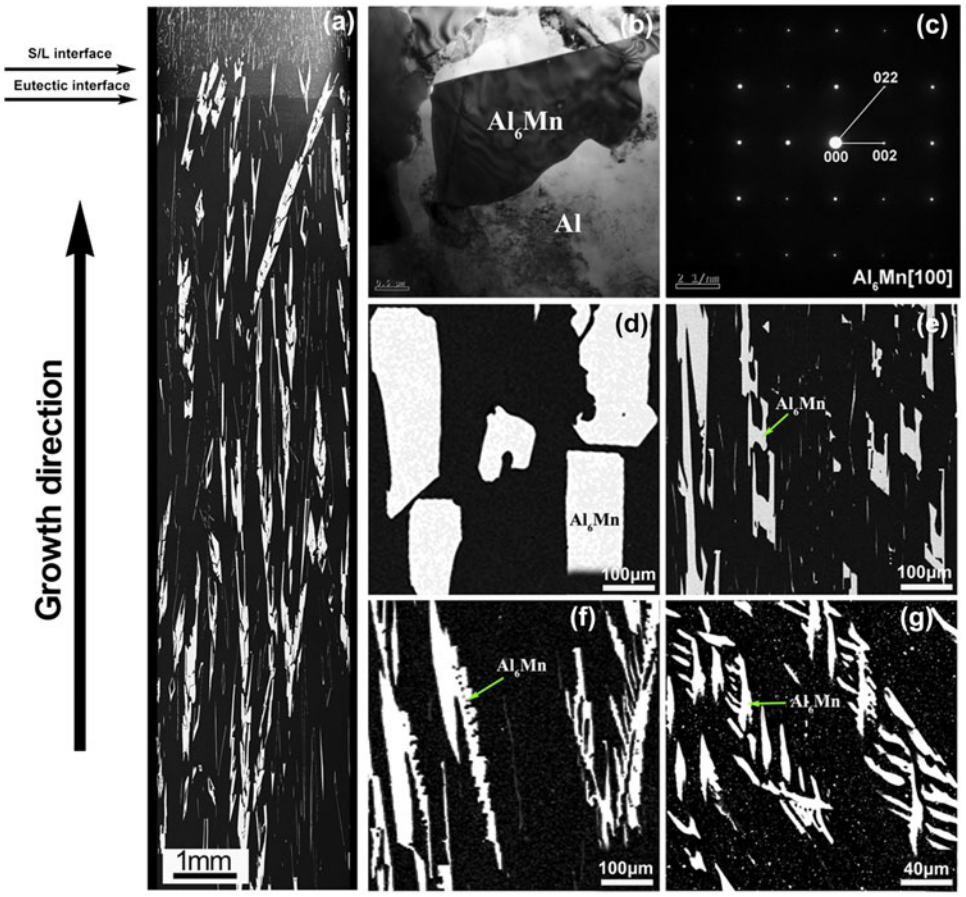

FIG. 1. Longitudinal structure (a), TEM bright field image (b) of directionally solidified Al–3 at.% Mn alloy at a growth rate of 10 μm/s, corresponding selected area electron diffraction pattern of Al_6Mn IMCs (c), and the typical SEM morphologies of primary Al_6Mn IMCs at selected growth rates: (d) 3 μm/s; (e) 20 μm/s; (f) 100 μm/s; (g)1000 μm/s.

c = 0.8681 nm.[18] Figures 1(d)–1(g) show the typical SEM morphologies of primary Al_6Mn IMCs at selected growth rates. With increasing growth rates, a morphological transition is observed from solid block [Fig. 1(d)] to V-shaped structure [Fig. 1(e)], and then to dendrites with slight arms [Fig. 1(f)] and finally dendrites with abundant arms [Fig. 1(g)]. This implies a faceted–nonfaceted growth transition. The decrease in sizes of primary Al_6Mn is also observed with increasing growth rates.

B. Three-dimensional morphology of Al_6Mn at various growth rates

For revealing the 3D morphologies of Al_6Mn IMCs, a deep etching technique was used by eliminating eutectic matrix. Figure 2(a) shows the 3D morphologies of primary Al_6Mn IMCs at 1 μm/s. Various solid truncated polyhedrons elongated in growth direction are observed. Most of Al_6Mn IMCs are found to form as "clusters" composed of series of 20–30 μm truncated polyhedrons, which were also observed in casting Al–Sc alloys at a slow cooling rate.[11] These polyhedrons own similar construction (indices) of crystal planes, but a slight difference in external morphologies, such as crystals (i) and (ii) marked in Fig. 2(a). It is attributed to growth discrepancies of different planes. Generally speaking, the final morphology of a crystal is mainly determined by both its intrinsic lattice structure and external conditions for growth.[7,9,19] The former determines the relative growth rates of various crystal planes which are significant for crystals with high entropy of fusion. And the latter includes solute concentration in melt, the direction of heat flow and solute rejected fields caused by competition growth between adjacent crystals, etc. Figure 2(b) shows the unit cell of Al_6Mn IMCs with an orthorhombic structure.[18] There are 28 atoms in a unit cell, including 4 manganese atoms and 24 aluminum atoms. Our previous work[8] reveals that (011) and (101) planes are the relatively close-packed planes and the growth direction is close to the [001] crystallographic direction at a low growth rate. So, the crystal-plane indices of the above polyhedrons can be deduced. For example, for an individual Al_6Mn crystal in Fig. 2(c), its Miller indices of

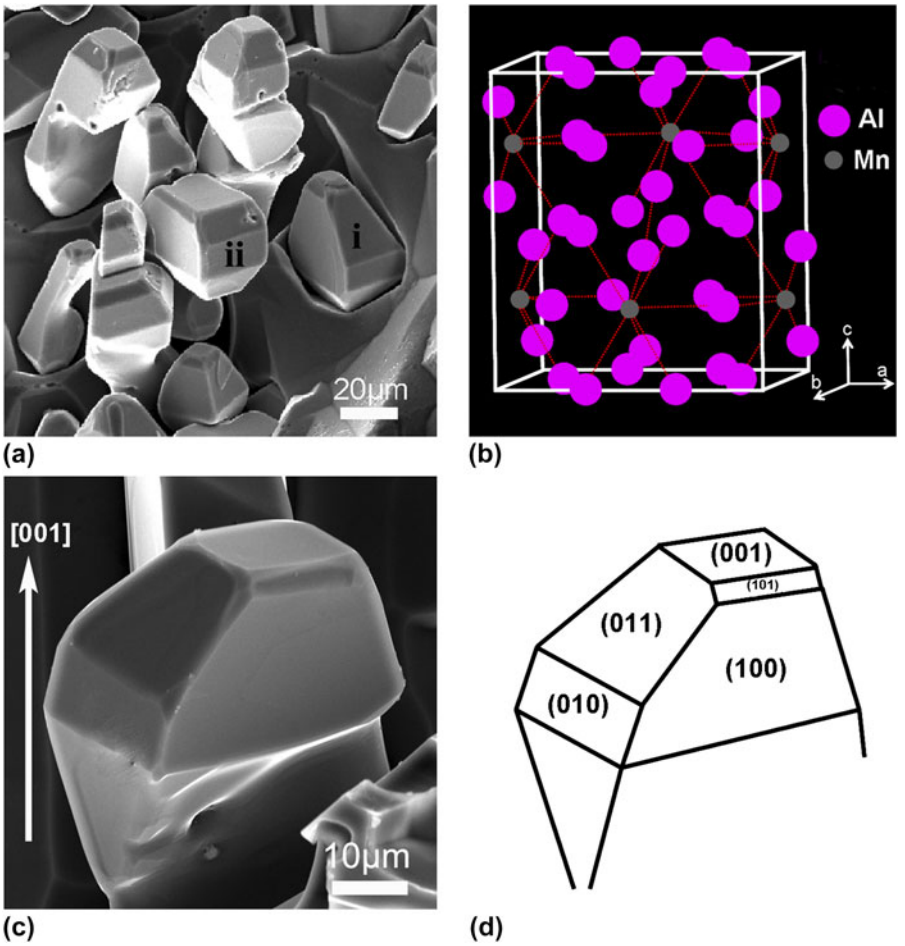

FIG. 2. 3D morphologies of primary Al_6Mn IMCs at 1 μm/s (a) and (c), unit cell of Al_6Mn IMCs (b), and indices of crystal planes corresponding to Fig. 2c (d).

planes are deduced, as shown in Fig. 2(d). Similar construction can be derived for other crystals. It suggests that these polyhedrons are bounded by {100} and {110} planes and the growth discrepancies of planes mainly affect external morphologies of polyhedrons.

Figure 3 shows the 3D morphologies of Al_6Mn IMCs at higher growth rates. With increasing growth rates, a morphological transition can be clearly observed from solid quadrangular prism [Fig. 3(a)], then to hollow quadrangular prism [Figs. 3(b) and 3(c)] and concave cylinder [Fig. 3(d)], and finally to dendrites [Figs. 3(e) and 3(f)], which is similar to what is observed for faceted snow crystals.[20] Again these results confirm a transition from faceted (lower than 60 μm/s) to nonfaceted growth (higher than 100 μm/s). A transient growth between them appears at growth rates of (60–100 μm/s). For example, at 100 μm/s, morphologies of both slim cylinder with surface pits and dendrites with slight arms are found. The mechanism of the growth transition is also observed for other faceted materials.[7,20,21] In addition, some growth details can be observed in Fig. 3, such as the large growth steps in insets of Figs. 3(a) and 3(b), and the growth-orientation change of secondary dendrite arms in insets of Figs. 3(e) and 3(f).

C. Mechanism of faceted–nonfaceted growth transition for Al_6Mn

Generally, crystal growth morphology results from the interplay of crystallographic anisotropy and growth kinetics. According to the thermodynamics principle of crystal growth and Wulff's theorem, the equilibrium crystal morphology results from minimizing the anisotropic surface free energy of a crystal under the constraint of constant volume.[22] Once a nucleus with its equilibrium shape is formed and the long-range transport is not an issue, it will grow toward its "kinetic Wulff shape", finally becoming bounded by surfaces of the more slowly growing orientations. For Al_6Mn IMCs, the "kinetic Wulff shape" should be the regular octahedron bounded by eight (011) and (101) planes. In fact, in many growth processes, long-range transport of heat or solute is important, or even dominant, such as the growth at fast growth rate. In this case, the morphological instabilities will be occurred due to the nature of long-range transport processes.[23] Therefore, for Al_6Mn IMCs, at a low growth rate (lower than 60 μm/s), the crystal morphology is mainly dictated by the anisotropies of interfacial energy and attachment kinetics (important for IMCs), leading to the formation of faceted morphology with sharp edges and corners, as shown in Figs. 3(a)–3(d). According to the Al–Mn binary diagram,[16] Al–3 at.% Mn alloy is a typical off-eutectic-type alloy ($k > 1$). During the growth of the Al_6Mn IMCs at a high growth rate (higher than 100 μm/s), the Al atoms are rejected into the melt, where it accumulates into Al boundary layer ahead of S/L interface. As a result, long-range diffusion of Al gives rise to the morphological instabilities of Al_6Mn IMCs at a high growth rate. In this case, small bulges appear at the edges and corners of the faceted Al_6Mn where the saturation attains its highest level, and protrude further into

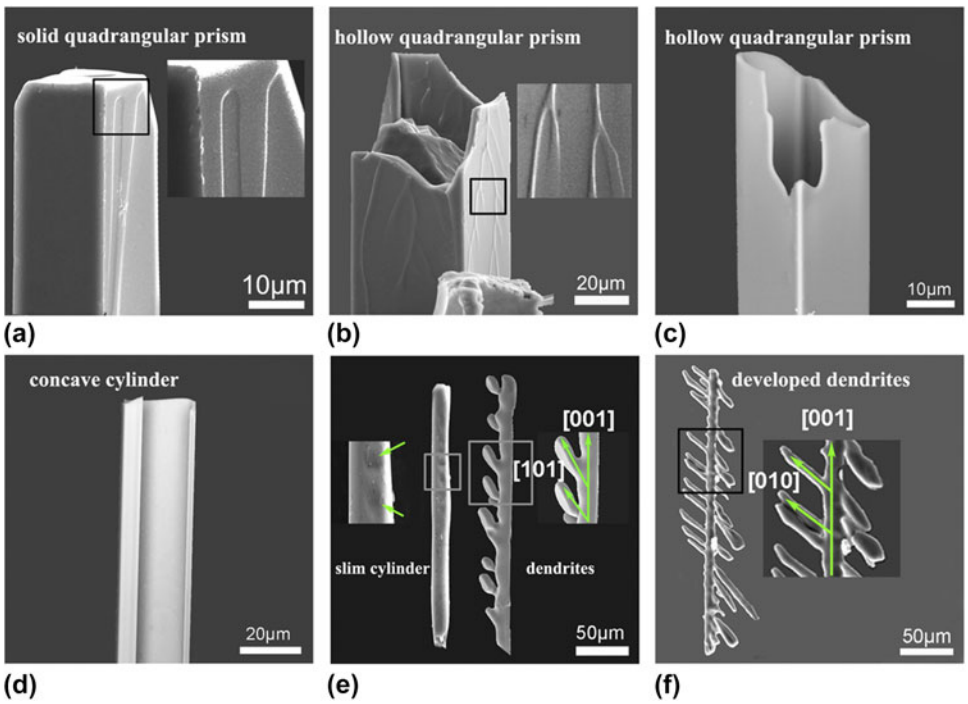

FIG. 3. 3D morphologies of Al_6Mn IMCs at various growth rates: (a) 3 μm/s; (b) 10 μm/s; (c) 20 μm/s; (d) 60 μm/s; (e) 100 μm/s; (f) 1000 μm/s. Inserts are enlarged images corresponding to the square areas drawn by solid lines.

the solute-rich regions. This process is self-sustained, and continuous growth of the branches leads to the formation of dendritic morphologies, as shown in Figs. 3(e) and 3(f). Finally, Al_6Mn IMCs undergo a faceted–nonfaceted growth transition as the growth rate increases.

In addition, to reveal the potential mechanism of the above faceted–nonfaceted growth transition in the process of directional solidification, detailed information about the kinetics of atom/cluster attachment to the solid/liquid (S/L) interface is needed during growth of Al_6Mn. For IMCs with a strict stoichiometric ratio like Al_6Mn, the S/L interface generally shows sharp shape with defined composition distribution. Thus, the atomic cluster in the liquid attachment to the S/L interface with same composition and structure is the major growth method.[24] Recently, Su et al. proposed a physical model of the faceted Al_2O_3/YAG eutectic growth based on the atomic cluster elementary process.[25] It can be improved to reveal the single-phase growth of IMCs, as shown in Fig. 4. Four representative regions (marked as 1, 2, 3, and 4) exist in the liquid ahead of the faceted interface. In region 1 next to the S/L interface, the liquid is composed of high density of large Al_6Mn-like clusters (name Al_6Mn-like clusters (Big/Small) as in Ref. 25) with same composition and structure. When the liquid is gradually far away from the S/L interface, small clusters are dominant, as shown in regions 2 and 3. In region 4 which is farthest away from S/L interface, the liquid is composed of completely mixed Al, Mn atoms or ions, and or their small clusters. When at a low growth rates (lower than V_1 in Fig. 4), the large clusters in region 1 stacking to the solid are enough to maintain the low-speed growth of the solid into the liquid. Furthermore, the inherently rough, high-index planes of the solid accept the large clusters readily and grow quickly relative to the low-index planes. Therefore, the S/L interface still remains sharp, and four regions in the liquid ahead of interface always exist to maintain such growth. The Al_6Mn IMCs show a faceted growth with a strong anisotropy. However, with increasing growth rates, both the large and small clusters (in regions 1 and 2, even 3) are needed to stack to the solid fast so that the solid reaches the growth rates growing into the liquid. This kind of stacking tends to be low selective to interfacial positions. Especially, plenty of clusters trapped by the interface (name cluster trapping) cause the S/L interface to be diffusive (rough), and weaken the growth discrepancies of planes. Typically at a critically high growth rate (V_3), complete cluster trapping happens, and only completely mixed region 4 exists in the liquid ahead of the diffusive interface. Therefore, under rapid solidification, the Al_6Mn IMCs shows a nonfaceted growth with dendritic morphologies.

D. 3D morphological evolution of Al_6Mn

As mentioned above, when growth rates are lower than 60 μm/s, primary Al_6Mn whose geometrical morphologies are mainly dominated by the competitions of different planes, shows a typical faceted growth. The competition is mainly determined by the anisotropies of interfacial energy and attachment kinetics. A relationship was built between growth morphologies and growth-rate ratios of different planes for many cubic crystals respectively by a geometric method based on the lattice parameters of their cubic structures.[12,26,27] Herein a similar work can be done for primary Al_6Mn. Due to the asymmetric lattice parameters ($a \neq b \neq c$) of Al_6Mn, the relationship is more complicated than that of cubic crystals. For simplicity, we mainly focus on three important planes of (001), (011), and (101) planes dominating the external shape of Al_6Mn (Fig. 2) and suppose $R_{(101)} = (D_{(101)}/D_{(011)})R_{(011)}$ and $D_{(101)}/D_{(011)} = 0.944$ except with special illustration, where $R_{(hkl)}$ is the growth rate of (hkl) plane and $D_{(hkl)}$ is the center-to-plane distance in a unit cell. In this case, (011) and (101) planes can be regarded as equivalent.

Figures 5(a)–5(d) schematically show the morphological evolution of Al_6Mn dependent on the growth-rate ratios of (001), (011), and (101) planes. If $R_{(001)}/R_{(101)} \leq 0.761$ and $R_{(001)}/R_{(011)} \leq 0.807$, Al_6Mn will grow as a perfect cubic.

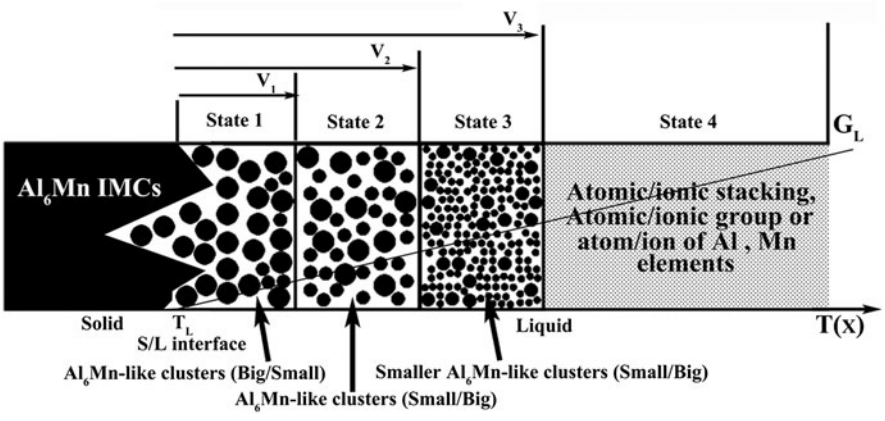

FIG. 4. A growth model of Al_6Mn IMCs based on the atomic cluster attachment.

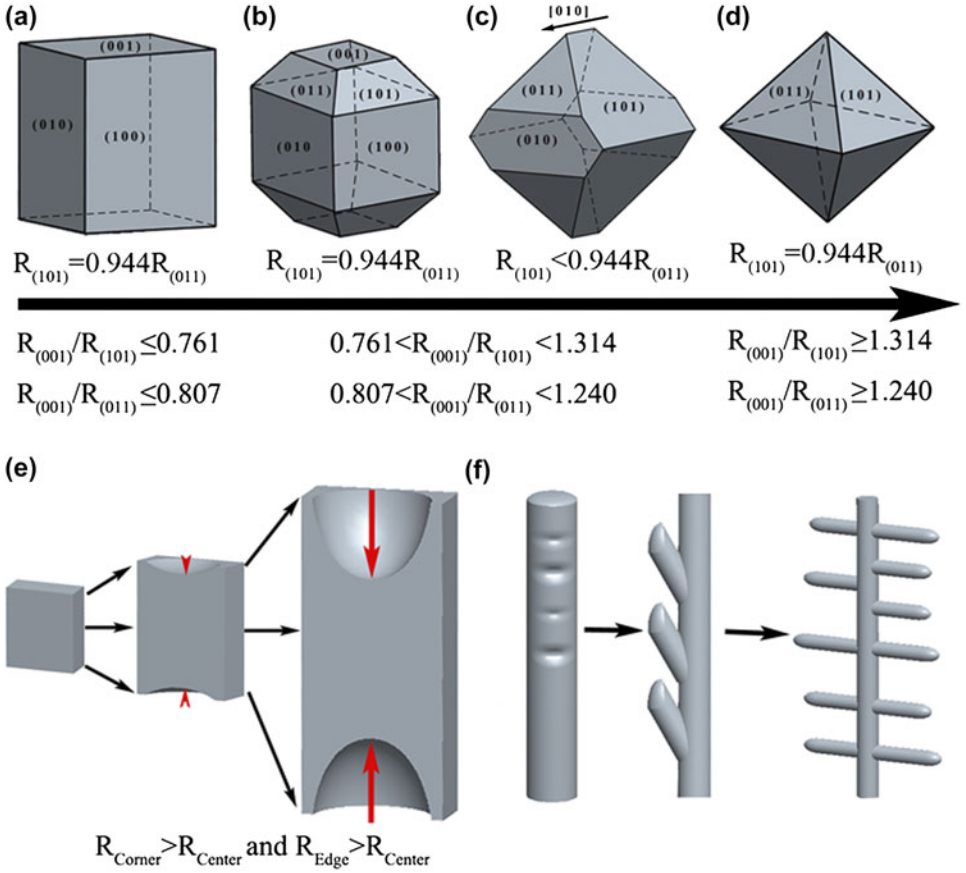

FIG. 5. Morphological evolution of Al_6Mn IMCs dependent on the growth-rate ratios of (001), (011), and (101) planes (a)–(d), schematic representations of the angular accelerated growth process (e) and a faceted–nonfaceted growth transition for Al_6Mn IMCs (f).

All {100} planes remain and {110} planes grow out, as shown in Fig. 5(a). When $0.761 < R_{(001)}/R_{(101)} < 1.314$ and $0.807 < R_{(001)}/R_{(011)} < 1.240$, {100} planes gradually shrink, but (011) and (101) planes appear, forming a truncated polyhedron bounded by (001), (011), and (101) planes, as shown in Fig. 5(b). This morphology is presented in Figs. 2(a) and 2(c). If $R_{(001)}/R_{(101)} > 1.314$ and $R_{(001)}/R_{(011)} > 1.240$, all {100} planes degenerate into corners and disappear, forming a perfect octahedron bounded by (011) and (101) planes, as shown in Fig. 5(d). The above analysis is based on the assumption of $R_{(101)} = 0.944R_{(011)}$, when $R_{(101)} < 0.944R_{(011)}$, $0.761 < R_{(001)}/R_{(101)} < 1.314$, and $0.807 < R_{(001)}/R_{(011)} < 1.240$, some {100} planes will degenerate into lines and ultimately disappear, as shown in Fig. 5(c). For example, the various polyhedrons in Fig. 2(a) fall in between that in Figs. 5(b) and 5(c). And the quadrangular prism in Fig. 3(a) falls in between that in Figs. 5(a) and 5(b) due to the gradually diminished {110} planes.

Increasing growth rates lead to an accelerated angular growth mechanism mainly determined by volume diffusion.[8,28] In this case, atoms (clusters) near edges and corners of crystals are easier to diffuse than that near the center of a plane. Therefore, compared to the center, the edges and corners have large growth rates, that is $R_{Corner} > R_{Center}$ and $R_{Edge} > R_{Center}$. Thus, a hollow quadrangular prism or concave cylinder appears [Figs. 3(b)–3(d)]. The growth process is schematically shown in Fig. 5(e). This kind of growth mechanism is also observed in other facet crystals.[7,12] However, further increasing growth rates lead to a large undercooling ahead of the S/L interface. When the degree of undercooling reaches the requirement of continuous growth, S/L interface becomes unstable and protrusions appear along the interface. As the growth proceeds, protrusions will be exaggerated and the Al_6Mn IMCs shows a nonfaceted growth with a dendritic morphology. Because of the effect of the solute gradient around the advancing tips of the first trunk, secondary dendrites are created along [110] or [100] directions [Figs. 3(e) and 3(f)]. Similar behavior also can be found in other faceted crystals.[7,29] In this case, the critical undercooling can be expressed as: $\Delta T^* = \pi\sigma g/\alpha$, where σ is the interfacial free energy and α is the step height.[30] For very diffuse boundaries, g is given approximately by $g = \pi x^3 \exp(-\pi x)$, where $x = n\pi/2$

and n is the number of atomic layers comprising the transition from solid to liquid at the melting temperature. As mentioned above, the growth of Al_6Mn IMCs is mainly dominated by long-range transport of heat or solute at a high growth rate (large n and g), small step height α and thus a large undercooling.[31] When the growth rate is higher than 100 μm/s, the critical undercooling can be reached for a nonfaceted growth of Al_6Mn IMCs in present experiments. Figure 5(f) schematically shows a potential process of faceted–nonfaceted growth transition for Al_6Mn IMCs. The preferred growth of (001) planes promotes the forming of a slim cylinder as observed in Fig. 3(e). Further accelerated growth leads to instability and then branching along [110] or [100] directions around the trunk.

IV. CONCLUSION

A transition from faceted (<60 μm/s) to nonfaceted (>100 μm/s) growth of primary Al_6Mn IMCs is observed with increasing growth rates. It is accompanied with the 3D morphological evolution of Al_6Mn from solid polyhedrons to hollow structure then dendrites. Increasing growth rates lead to an accelerated angular growth mechanism mainly determined by volume diffusion, resulting in hollow structures. Further increasing growth rates lead to a large undercooling ahead of the S/L interface, continuous growth of Al_6Mn IMCs occurs, and a nonfaceted growth of Al_6Mn IMCs with dendritic morphologies appears. A growth model based on atomic cluster attachment is proposed to reveal the faceted–nonfaceted growth transition. A large growth rate leads to cluster trapping and forming a diffusive interface, driven by the large undercooling ahead of the interface. Thus a nonfaceted growth of Al_6Mn IMCs with dendritic morphologies appears. Moreover, as for faceted growth, a relationship between 3D morphologies and growth discrepancies of crystal planes has been built.

ACKNOWLEDGMENTS

This project was supported by the National Natural Science Foundation of China (Nos. 51271068, 51274077, 51274054, U1332115), the key grant project of Chinese Ministry of Education (No. 313011), the China Postdoctoral Science Foundation (No. 082090), and the Fundamental Research Funds for the Central Universities.

REFERENCES

1. N.S. Stoloff, C.T. Liu, and S.C. Deevi: Emerging applications of intermetallics. *Intermetallics* **8**, 1313 (2000).
2. R.J. Contieri, E.S.N. Lopes, M. Taquire de La Cruz, A.M. Costa, C.R.M. Afonso, and R. Caram: Microstructure of directionally solidified Ti–Fe eutectic alloy with low interstitial and high mechanical strength. *J. Cryst. Growth* **333**, 40 (2011).
3. L. Li, Z. Zhao, Y. Zuo, Q. Zhu, and J. Cui: Effect of a high magnetic field on the morphological and crystallographic features of primary Al_6Mn phase formed during solidification process. *J. Mater. Res.* **28**, 1567 (2013).
4. H. Kaya, S. Engin, U. Böyük, E. Çadırlı, and N. Maraşl&imath: Unidirectional solidification of Zn-rich Zn–Cu hypoperitectic alloy. *J. Mater. Res.* **24**, 3422 (2009).
5. B.P. Bewlay and M.R. Jackson: The effect of Hf and Ti additions on microstructure and properties of Cr2Nb–Nb in situ composites. *J. Mater. Res.* **11**, 1917 (1996).
6. S. Wang, L. Luo, Y. Su, J. Guo, and H. Fu: A lateral remelting phenomenon of the primary phase below the temperature of peritectic reaction in directionally solidified Cu–Ge alloys. *J. Mater. Res.* **28**, 3261 (2013).
7. C. Li, Y.Y. Wu, H. Li, and X.F. Liu: Morphological evolution and growth mechanism of primary Mg_2Si phase in Al–Mg_2Si alloys. *Acta Mater.* **59**, 1058 (2011).
8. H. Kang, X. Li, Y. Su, D. Liu, J. Guo, and H. Fu: 3-D morphology and growth mechanism of primary Al_6Mn intermetallic compound in directionally solidified Al-3at.% Mn alloy. *Intermetallics* **23**, 32 (2012).
9. W. Kurz and D.J. Fisher: *Fundamentals of Solidification* (Trans Tech Publications Ltd., Switzerland, 1998); pp. 21–41.
10. H. Kang, X. Li, T. Wang, D. Liu, Y. Su, Z. Hu, J. Guo, and H. Fu: Crystal–quasicrystal transition depending on cooling rates in directionally solidified Al–3Mn–7Be (at.%) alloy. *Intermetallics* **44**, 101 (2014).
11. K.B. Hyde, A.F. Norman, and P.B. Prangnell: The effect of cooling rate on the morphology of primary Al_3Sc intermetallic particles in Al–Sc alloys. *Acta Mater.* **49**, 1327 (2001).
12. R.Y. Wang, W.H. Lu, and L.M. Hogan: Growth morphology of primary silicon in cast Al–Si alloys and the mechanism of concentric growth. *J. Cryst. Growth* **207**, 43 (1999).
13. Y. Chen and H.M. Wang: Growth morphologies and mechanisms of non-equilibrium solidified MC carbide. *J. Mater. Res.* **21**, 375 (2006).
14. C. Deppisch, G. Liu, A. Hall, Y. Xu, A. Zangvil, J.K. Shang, and J. Economy: The crystallization and growth of AlB2 single crystal flakes in aluminum. *J. Mater. Res.* **13**, 3485 (1998).
15. J. Fu and Y. Yang: Crystallography and morphology of a lathy ferrite in Fe–Cr–Ni alloys during directional solidification. *J. Mater. Res.* **28**, 2040 (2013).
16. Å. Jansson: A thermodynamic evaluation of the Al–Mn system. *Metall. Mater. Trans. A* **23**, 2953 (1992).
17. D. Liu, X. Li, Y. Su, L. Luo, J. Guo, and H. Fu: Solute redistribution during planar growth of intermetallic compound with nil solubility. *Intermetallics* **26**, 131 (2012).
18. K. Yamamoto and Y. Matsuo: X-ray study of the electron density distribution for Al_6Mn. *J. Phys.: Condens. Matter* **12**, 2359 (2000).
19. J. Nie, Y. Wu, P. Li, H. Li, and X. Liu: Morphological evolution of TiC from octahedron to cube induced by elemental nickel. *CrystEngComm* **14**, 2213 (2012).
20. G.L. Kenneth: The physics of snow crystals. *Rep. Prog. Phys.* **68**, 855 (2005).
21. S.M. Li, Q.R. Quan, X.L. Li, and H.Z. Fu: Increasing the growth velocity of coupled eutectics in directional solidification of off-eutectic alloys. *J. Cryst. Growth* **314**, 279 (2011).
22. R.L. Dobrushin, R. Kotecý, and S. Shlosman: *Wulff construction: A Global shape from Local Interaction* (American Mathematical Society, Providence, RI, 1992); pp. 1–20.
23. R.F. Sekerka: Theory of crystal growth morphology. In *Crystal Growth – From Fundamentals to Technology*, G. Müller, J.J. Métois, and P. Rudolph eds.; Elsevier Science B.V., Amsterdam, Netherlands, 2004; pp. 55–93.
24. Y. Waku, N. Nakagawa, T. Wakamoto, H. Ohtsubo, K. Shimizu, and Y. Kohtoku: A ductile ceramic eutectic composite with high strength at 1,873 K. *Nature* **389**, 49 (1997).

25. H.J. Su, J. Zhang, L. Liu, J. Eckert, and H.Z. Fu: Rapid growth and formation mechanism of ultrafine structural oxide eutectic ceramics by laser direct forming. *Appl. Phys. Lett.* **99**, 221913 (2011).
26. Z.L. Wang: Transmission electron microscopy of shape-controlled nanocrystals and their assemblies. *J. Phys. Chem. B* **104**, 1153 (2000).
27. S. Jin, P. Shen, B. Zou, and Q. Jiang: Morphology evolution of TiC_x grains during SHS in an Al–Ti–C system. *Cryst. Growth Des.* **9**, 646 (2009).
28. G. Bögels, J.G. Buijnsters, S.A.C. Verhaegen, H. Meekes, P. Bennema, and D. Bollen: Morphology and growth mechanism of multiply twinned AgBr and AgCl needle crystals. *J. Cryst. Growth* **203**, 554 (1999).
29. C.L. Xu, H.Y. Wang, C. Liu, and Q.C. Jiang: Growth of octahedral primary silicon in cast hypereutectic Al–Si alloys. *J. Cryst. Growth* **291**, 540 (2006).
30. J.W. Cahn, W.B. Hillig, and G.W. Sears: The molecular mechanism of solidification. *Acta Metall.* **12**, 1421 (1964).
31. J.Q. Broughton, G.H. Gilmer, and K.A. Jackson: Crystallization rates of a Lennard-Jones liquid. *Phys. Rev. Lett.* **49**, 1496 (1982).